Numerical spatio-temporal characterization of *Listeria monocytogenes* biofilms

M. Mosquera-Fernández, P. Rodríguez-López, M. L. Cabo, E. Balsa-Canto*

Instituto de Investigaciones Marinas (CSIC), C/ Eduardo Cabello 16, E-36208, Vigo (Pontevedra) Spain. Authors E-mail address: maruxamosquera@iim.csic.es (M. Mosquera-Fernández), pedrorodriguez@iim.csic.es (P. Rodríguez-López), marta@iim.csic.es (M.L.Cabo) and ebalsa@iim.csic.es (E. Balsa-Canto)

*Corresponding author E. Balsa-Canto, C/ Eduardo Cabello 16, E-36208, Vigo (Pontevedra) Spain, e-mail address: ebalsa@iim.csic.es and phone number: +34 986 231930 ext. 403.

Abstract

As the structure of biofilms plays a key role in their resistance and persistence, this work presents for the first time the numerical characterization of the temporal evolution of biofilm structures formed by three *Listeria monocytogenes* strains on two types of stainless-steel supports, AISI 304 SS No. 2B and AISI 316 SS No. 2R.

Counting methods, motility tests, fluorescence microscopy and image analysis were combined to study the dynamic evolution of biofilm formation and structure. Image analysis was performed with several well-known parameters as well as a newly defined parameter to quantify spatio-temporal distribution.

The results confirm the interstrain variability of *L. monocytogenes* species regarding to biofilm structure and structural evolution. Two types of biofilm were observed: homogeneous or flat and heterogeneous or clustered. Differences in clusters and in attachment and detachment processes were due mainly to the topography and composition of the two surfaces although an effect due to motility was also found.

Keywords: *L. monocytogenes*, biofilm, image analysis, structure, stainless steel

1. INTRODUCTION

In United States, 2011-2014, 183 persons were infected with the outbreak-associated strain of *Listeria monocytogenes*, resulting 39 deaths. Such infections were associated with food, in particular, with three different cheese brands and cantaloupe (CDC, 2014). In Europe eight strong-evidence food-borne outbreaks caused by *L. monocytogenes* were reported among 2011-2012 (ECDC and EFSA, 2013; ECDC and EFSA, 2014). The outbreaks resulted in 71 cases and 9 deaths. The implicated foods were sandwiches, bakery products, meat and cheese. Miettinen et al., (1999) showed the persistence ability of *L. monocytogenes* in an ice-cream plant during 7 years. This reflects the relevance of biofilms for the food industry (Moretro and Langsrud, 2004) and identifies *L. monocytogenes* as a major concern.

Because of this, a complete cost-effective cleaning procedure and sanitizer protocols are essential to avoid recontamination of food surfaces and food products by the spread of biofilm-dwelling microorganisms after detachment promoted by the dynamic nature of biofilms (Chavant et al., 2002). In this concern, quantification of the biofilm structure of pathogenic bacterial species is of the highest interest and knowledge of intrastrain variations is basic for understanding biofilm behaviour and designing adequate disinfection techniques.

A number of studies of materials commonly used in food facilities and premises have shown the presence of *L. monocytogenes* (Moreto and Langsrud, 2004; Sofos, 2008), demonstrating the ability of *L. monocytogenes* to adhere and develop on various food-contact surfaces, such as polystyrene (Silva et al., 2008) used e.g. as construction material in floor drains; polytetrafluoroethylene, PTFE, (Chavant et al., 2002) used in conveyor belts; stainless steel (Kalmokoff et al., 2001) used in smokehouses; polyester (Blackman and Frank, 1996) used as a floor sealant or rubber (Ronner and Wong, 1993) used in gaskets and glass (Borucki et al., 2003). Remark that the degree to which *L. monocytogenes* attaches to these materials differs.

The degrees to which cells initially attach to a surface and the amount of biofilm produced have been studied by indirect and direct methods (Djordjevic et al., 2002). In indirect methods, the number of cells *in situ* is estimated in specific assays, such as crystal violet staining on a microtiter plate (Stepanovic´ et al., 2000), enzyme-linked immunosorbent assays (Wakimoto et al., 2004), polymerase chain reaction (Lau et al., 2004) and denaturing gradient gel electrophoresis analysis (An and Friedman, 2000), in which the intensity of the response correlates with attached cells density. In some indirect methods the biofilms are disrupted by mechanical procedures such as vortexing, sonication and scraping before cells are counted. Direct methods are imaging techniques such as epifluorescence, atomic force (ATM), electronic (SEM) and confocal microscopies (CLSM). Some of these techniques allow direct quantification of the number and location of cells within biofilms, cell size and morphology (Daims and Wagner, 2007), the viability of cells (Twakoli et al., 2013), the amount of extracellular polymeric substance and its distribution and three-dimensional reconstruction of the biofilms (Zang and Fang, 2001) and the phylogenetic composition of bacteria (Manz et al., 1999).

Yang et al., (2000) proposed a set of two-dimensional structural parameters for the characterization of biofilms concluding, however, that areal porosity (AP) and maximum and average diffusion distances (ADD and MDD) are the most useful parameters of those studied (Beyenal et al., 2004), as they are easily interpreted and related. In the same line, Heydorn et al. (2000a) recommended the selection, depending on the aim of the study, of the smallest set of reasonable parameters.

The formation of biofilms by *L. monocytogenes* has been widely investigated. Most studies have addressed cell density or biomass production of biofilms (Djordjevic et al., 2002; Kalmokoff et al., 2001; Rodríguez et al., 2008) and qualitative structural descriptions of biofilms under different conditions (see for example, Bremer et al., 2002; Carpentier and Chassaing, 2004; Djordjevic et al., 2002; Marsh et al., 2003, Perni et al., 2007). Chae and Schraft (2000) reported evolution of the thickness of *L. monocytogenes* Murray and 7148 biofilms over 2-4 days.

However, surprisingly few experimental studies have been performed in order to numerically characterize biofilm structure of *L. monocytogenes* and to establish numerical differences among strains. In addition, the dynamic nature of the structure formation has not been considered. Bridier et al. (2010) reported the biovolume, maximum thickness, substratum coverage and roughness at 24 h of biofilms produced by 10 *L. monocytogenes* strains, no further dynamic studies were performed. Chae and Schraft (2000) reported thickness values at only two times during biofilm development (48h and 96h) in order to observe interstrain differences. Rieu et al. (2008) studied the evolution of biovolume and thickness for up to 48 h of maturation of biofilms produced by *L.monocytogenes* AR009 strain. Again only 3 sampling times were considered given only limited information about the dynamics.

This work moves a step forward and considers, for the first time, the dynamic evolution of the formation of biofilms by *L. monocytogenes*. A comparative study of the structure formation of three strains on two types of stainless-steel food-contact surfaces was performed. Two types of biofilms were observed: homogeneous or flat and heterogeneous or clustered. Differences in clusters and in attachment and detachment processes were due mainly to the topography and composition of the two surfaces although an effect due to motility was also found.

2. MATERIALS AND METHODS

2.1 Microorganism, media and culture conditions

Three *L. monocytogenes* strains CECT 4032 (from soft cheese, serotype 4b and lineage I) and CECT 5878 (from guinea-pig, serotype 1/2a and lineage II) were obtained from the Spanish Type Culture Collection (Microbial Resource Centre, University of Valencia, Spain and L1.A1 (serotype 1/2a/3a, lineage II) was isolated from thermal gloves used in the fishing industry by the Microbiology and Marine Technology Products research group at our institute.

The strains were frozen and stored at –80 ˚C in Tryptone Soy Broth medium (TSB, Cultimed, S.L., Spain) containing 50% glycerol in the ratio 1:1 (v/v) until use. For each experiment, strains were grown in consecutive subcultures on tryptone soy broth medium (Cultimed, Spain) for 24–48 h at 37 ˚C. Volume ratios of inoculum to broth medium of 1:5 and 1:50 were tested for each subculture. Erlenmeyer flasks containing 35 ml broth medium were inoculated with 5 ml of 48-h cultures to obtain a final absorbance at

700 nm of 0.1 (± 0.001), which corresponds to about 10^8 CFU/ml according to a previous calibration. These cell suspensions were used directly as the inoculum for subsequent biofilm formation.

2.2 Motility test

The motility of cells was determined by swimming tests. Four different test media were prepared from 25g/L of Lysogeny Broth (BD Difco, USA) with different concentrations of Agar (BD Difco, USA): 0.15%, 0.20%, 0.25% and 0.30%. 25ml of semisolid medium previously dispensed into a culture plate were stabbed with a sterile needle containing an inoculum of *L. monocytogenes* strain. Plates were incubated at 25ºC. Diameters of cells dispersion (µm) were measured after 24h, 48h and 72h from incubation. Six replicates were performed.

2.3 Biofilm formation

Both 304 and 316 austenitic stainless steel coupons were chosen as work surfaces in this study. These two grades are widely used in the food and beverage industry as food contact material for transportation; processing equipment, e.g. in the dairy, fruits, vegetables, cereals industries; for containers such a wine tanks, for brew kettles and beer kegs or for utensils such as blenders and bread dough mixers, to name a few (Heubner, 2009).

Two diverse grade and finish were tested: AISI 304 (L) SS, No 2B characterized, according to manufacture measurements (Acerinox, Spain), by an average roughness (Ra) value ranged between 0.05-0.15 and AISI 316 (L) SS, No 2R characterized by Ra value ranged between 0.03-0.06. In contrast with the other type, AISI 316 stainless steel presents Molybdenum (Mo). Stainless-steel surface topography was examined by SEM, and each surface was cut into squares (1 x 1 cm) 1 mm thick. The squares were pre-treated before culture by immersing them in 96% ethanol solution.

Cleaned squares were placed in 24-well flat-bottomed microtitre plates and inoculated with 1 ml of active liquid culture (10^8 CFU/ml) of each *L. monocytogenes* strain. The microplates were incubated at 25 ˚C under static conditions for biofilm formation until harvesting at 24-h intervals and double sampling. Samples were taken from both support types at 72–312 h on AISI 304 SS and at 24–240 h on AISI 316 SS.

2.4 Number of adherent cells

The number of adherent cells was determined according to Herrera et al. (2007). Samples were collected at 24, 72, 120, 168 and 216 h from squares removed from the microtitre cavities and immersed in 10 ml of phosphate-buffered saline for 10 s to release non-adherent cells. Adherent cells were collected with peptone water-moistened swabs. After the squares had been rubbed twice with the swabs, they were transferred to 10 ml peptone water and subjected to 1 min of vortexing. The number of adherent cells was determined by plating the appropriated serial dilutions on tryptic soy agar (Cultimed, Spain) after incubation at 37 ˚C for 24 h. Outcomes are expressed as log CFU/cm^2.

2.5 Epifluorescence microscopy

Squares with attached cells were rinsed in 1 ml of 0.05 M phosphate buffered saline for 10 s to release non-adherent cells. FilmTracer™ calcein green biofilm fluorochrome (Invitrogen, USA) was used as the stain according to the manufacturer's instructions. This fluorochrome labels only viable cells in green after laser excitation (490 nm), excitation emitted by cells (524 nm) and capture by the microscope detector. This labelling method was chosen because it is non-invasive, allowing visualization of biofilms *in vivo* without losing the structure information. We visualized and captured digital images with a LEICA (DM4500P) epifluorescence microscope from 10 fields per square with a 40x objective.

2.6 Image analysis

Each image was pre-processed, analysed and post-processed with a MATLAB-based code, BIOFILMDIVER, which we developed to perform dynamic analyses and to process several strains in parallel. The image parameters computed were AP, ADD, MDD designed by (Yang et al., 2000), covered area (CA) and the spatio-temporal population distribution (STPD). Details on the computation of the different parameters are reported in the supplementary data (section 1); a brief description is presented here.

AP is the ratio between the number of void pixels and the total number of pixels, the actual area of the pixel is used to compute covered area; ADD and MDD reflect the mean and maximum distances covered by cells. We also calculated a new structural parameter, the spatio-temporal population distribution (STPD), which represents the temporal evolution of the projection of the number of green pixels over one spatial axis.

For each sampling time, 10 images were selected to compute the parameter values by the representative elementary area method (Korber el al., 1993; Ma and Bryers, 2010). The results are depicted as boxplots to show explicitly the differences between images of the same square and replicates.

3. RESULTS

3.1 Motility test results

Motility test results revealed all strains studied are motile as shown in Figure 1. However remarkable differences among strains were observed. CECT 4032 strain was the most motile whereas L1.A1 strain was the less motile. Note that after 72h CECT 4032 strain has moved around twice the distance than L1.A1 strain.

3.2 SEM of stainless-steel squares

SEM of the two support types showed different topographies. The surface of AISI 304 SS No2B was characterized by grainy boundaries due to the pickling treatment. These boundaries consisted of concave clefts, generating pseudo-geometric forms (Figure 2A). Micrographs of the AISI 316 SS No.2R surface displayed smooth crevices (Figure 2B), with zones in which the crevices were more common and deeper.

3.3 Plate count results

Results showed the same range of adhered cell counts (between 6 and 8.5 log CFU/cm^2) in all cases. Remarkably a delay in the adherence is observed in AISI 316 SS. Detailed results may be found in the supplementary data (section 2).

3.4 Epifluorescence microscopy images

Visual inspection of the images revealed two structural spatio-temporal patterns, with a characteristic pattern for L1.A1strain, which was conserved in both surfaces, and a different pattern for CECT 4032 and CECT 5873 strains, also in both surfaces. The L1.A1 strain formed dense biofilms that covered the entire surface. After the initial sampling, when the cells were randomly distributed over the surface, the biofilm evolved from a net-like pattern to a homogeneous layer of cells covering the surface. After maximum coverage (at 120 h), a sharp decrease in adhered cells was observed. Representative images are shown in Figure 3 (A, B, C). CECT 4032 and CECT 5873 strains did not form dense biofilms. The individual cells initially distributed randomly on the surface evolved to form cell aggregates or clusters that disappeared later (Figure 3 (D, E, F) and Figure 3 (G, H, I)).

3.5 Quantitative image analysis

3.5.1 L1.A1 strain

The L1.A1 image parameters (AP, ADD, MDD, CA and STPD) suggested a dynamic profile characterized by the presence of peaks at 120 h for AISI 304 SS and 168 h for AISI 316 SS, although the magnitude of the peak differed. The parameters for AISI 304 SS were significantly higher than for AISI 316 SS, except for the AP. The AP value for AISI 304 SS was in the range around 0.69–0.99, whereas that for AISI 316 SS was narrower (0.87–0.99) (Figure 4, A, B). The maximum percentage of covered area for AISI 304 SS was about 40% but no more than 13% for AISI 316 SS (Figure 4, C, D). The ADD was within the range 1.75–2.8 for AISI 304 SS and almost constant around 1 for AISI 316 SS (Figure 4, E, F). The MDD achieved a maximum of around 17 for AISI 304 SS and about 4.2 for AISI 316 SS (Figure 4, G, H).

Figure 5 shows the STPD on AISI 304 SS and AISI 316 SS, indicating that L1.A1 cells adhere and occupy the entire surface simultaneously until they reach a maximum value of occupation (at 120 h). Cells also detach simultaneously at all positions on the surface, so that the number of viable cells is similar at all sites at a given time. Replicas grown in same austenitic grade (304L or 316L) achieved

198 similar STPD profiles, with slight variations in the number of viable cells. The peaks were delayed by
199 48 h on one surface with respect to the other as observed in cell counts.

200 **3.5.2 CECT 4032 strain**

201 The CECT 4032 image parameters suggested a dynamic profile characterized by the presence of various
202 peaks, which differed according to the support, as observed for the L1.A1 strain. The AP was similar on
203 the two surfaces, ranging from 0.94 to 1 (Figure 6, A, B). As expected, the covered area was also similar
204 (Figure 6, C, D), reaching values of 13%. Large differences were found in ADD and MDD, with peak
205 profiles for both parameters on both supports although the magnitude, number and location of the peaks
206 varied (Figure 6, E, H).

207 Figure 7 shows the STPD of CECT 4032 strain on AISI 304 SS and AISI 316SS. This strain had a highly
208 heterogeneous distribution, with two peaks for each surface. The delay between peaks observed with
209 L1.A1 strain was also observed for this strain.

210 **3.5.3 CECT 5873 strain**

211 The CECT 5873 image parameters suggested a dynamic profile similar to that observed for CECT 4032
212 strain, with the presence of several peaks of different heights in the squares. The AP was 0.99–1 for AISI
213 304 SS and 0.98–1 for AISI 316 SS (Figure 8, A, B). The percentage of covered area was more sensitive
214 to changes but was smaller on both supports (0.2–2.4%) than with the other strains (Figure 8, C, D).

215 Figure 9 shows the STPD of CECT 5873 strain on AISI 304 SS and AISI 316 SS, indicating highly
216 heterogeneous distribution. Several peaks were observed over time on both surfaces. The presence of
217 isolated peaks indicates the presence of larger aggregations than with CECT 4032 strain.

218 **4. DISCUSSION**

219 The temporal evolution of the structure of the biofilms formed by the three *L. monocytogenes* strains was
220 largely conditioned by early-stage adhesion. Under our experimental conditions, a batch system with no
221 nutrient renewal and planktonic cells in a stationary stage, it would be expected that biofilm formation
222 occurs mainly by cell deposition on surfaces. Under this hypothesis, cell deposition is due mainly to
223 mechanical forces (Takhistov and George, 2004), whereas cell adherence is conditioned mainly by
224 electrostatic interactions (λ) and short-range attraction energy (E) (Ivanenko et al., 1999).

225 In addition to these physical forces, cell distribution on surface is affected by the surface topography. The
226 topography of AISI 304 SS (Figure 10A), characterized by pseudo-geometric figures formed by deep
227 clefts induced during pickling, promotes cell entrapment at early stages of biofilm formation. This may be
228 due to the increase in binding energy caused by the increased microbe–surface contact area (Edwards and
229 Rutenberg, 2001). The effect can be seen in Figure 10B, where cells form chains along the grainy
230 boundary. Similar net-like patterns have been observed previously for *L. monocytogenes* and other
231 bacteria (Verran et al., 2001; Djordjevic et al., 2002; Marsh et al., 2003). AISI 316 SS presented a
232 smoother surface (Figure 2B); therefore, biofilm structure evolution was driven by other factors
233 (Vatanyoopaisarn et al., 2000; Kalmokoff et al., 2001; Lundén et al., 2000; Todhanakasem and Young,
234 2008). Clear differences in L1.A1 structures on the two supports can be seen in Figure 10.

235 Accumulation of cells in clefts induces the formation of microcolonies, either because the cells divide and
236 stay together or because they tend to accumulate in the same crevices (Marsh et al., 2003; Takhistov and
237 George, 2004). This would explain the higher ADD and MDD values obtained for all strains on AISI 304
238 SS than on AISI 316 SS, showed in Figure 4 (E, G), Figure 6 (E, G) and Figure 8 (E, G).

239 Entrapment might be reduced by cell motility; this would partially explain the differences in distribution
240 and population observed among the strains with different motilities. L1.A1 strain tended to develop flat
241 biofilms (Figure 3B), whereas CECT 4032 and CECT 5873 strains tended to move and develop cell
242 aggregates or clusters (Figure 3E and Figure 3H).

243 Coupon topography differences and the presence of molybdenum - with proved antibacterial properties
244 (Guggenbichler et al, 2007) - in AISI 316 SS, may explain the delay experienced in the biofilm formation
245 observed in AISI 316 SS with respect to AISI 304 SS.

Differences in biofilms on the two supports could be also related to variations in the growth rate of strains and in random initial cell deposition. Two main biofilm formation patterns were observed. The L1.A1 strain had a characteristic homogeneous distribution of viable cells over the support, with cells that appeared to attach and detach from the surface simultaneously. The ADD and MDD values Figure 4 (E, F, G, H), confirm the wrap-like distribution indicated by STPD (Figure 5). The patterns formed by CECT 4032 and CECT 5873 strains, however, had high AP values and low covered area as Figure 6 (A, B, C, D) and Figure 8 (A, B, C, D) show, indicating lower population levels (in terms of viable cells) than for the L1.A1 strain. The high ADD and MDD values and STPD profile, showed in Figure 6 (E, F, G, H), Figure 8 (E, F, G, H), Figure 7 and Figure 9; indicate that these two Listeria strains form clusters surrounded by individual viable cells.

The dynamic evolution of the parameters for CECT 4032 and CECT 5873 also differed from that for L1.A1 strain. The single peak shown by the L1.A1 strain implies a unique episode of attachment and a unique episode of detachment, while for CECT 4032 and CECT 5873 strains several episodes of attachment–detachment were observed. Similar behaviour was observed for biofilm formation of *L. monocytogenes* LO28 on stainless steel by Chavant et al. (2002) or even in other microorganisms, such as *Pseudomonas* (Heydorn et al, 2000b). Todhanakasem and Young (2008) discussed the possible relation between population level oscillations and the motility of *L. monocytogenes* strains.

Although plate counts are typically used to analyse biofilm formation, we found several discrepancies between plate counts and image analysis. Changes in cluster size or even the presence of clusters observed with the CECT 4032 and CECT 5873 strains would not have been predicted from the corresponding plate counts. In addition, AP and covered area do not correspond to the dynamic profiles of plate counts. Use of plate counts may be misleading in the evaluation of the progress of biofilms (Daims and Wagner, 2007), as it includes only viable culturable cells, whereas in imaging viable and viable non-culturable cells are taken into account.

Remark that a quantitative comparison of the results achieved with counting and image analysis techniques is not straightforward. This may be partially explained by the fact that counting methods consider viable culturable cells, whereas imaging considers culturable and non-culturable and the possible overestimation of epifluorescence techniques due to the well-known out-of-focus bur.

Nevertheless, not all image-related parameters provide the same amount or quality of information. We found that AP is less sensitive to changes than the covered area parameter, which may be related to the fact that the number of pixels is used to compute the AP while area is used to compute the covered area. This resulted in different ranges of values; for example, the AP (Figure 4A) was 0.42–1, while the covered area (Figure 4C) was 0–59 for L1.A1 strain and the AP (Figure 8A) was 0.95–1 while the covered area (Figure 8C) was 0–5.5 for CECT 5873 strain. In addition, large differences between MDD and ADD reflect the presence of large clusters; for example, L1.A1 strain had higher MDD and ADD values than the other strains, as Figure 4 (E, F, G, H), Figure 6 (E, F, G, H) and Figure 8 (E, F, G, H) shows; but this does not mean that L1.A1 strain formed clusters, as seen from the STPD profile in Figure 5 (homogeneous spatial distribution for L1.A1 strain and peak spatial distributions for the other strains). The MDD appeared to correspond to the smoother topography of stainless steel AISI 316, as its values were almost constant around 1, indicating homogeneous distribution of cells or small cell aggregations (Figure 4H, Figure 6H and Figure 8H). We conclude that a combination of MDD, covered area and STPD provides the right information to determine biofilm structure from 2D images.

5. CONCLUSIONS

We have characterized the evolution of biofilm structure by three *L. monocytogenes* strains in two stainless-steel supports. Fluorescence image analysis, motility tests and plate counting were used to identify the key elements of the structures generated by each strain.

The results confirm the expected interstrain variability of this species, with two patterns observed: flat biofilms with L1.A1 strain and clustered biofilms with CETC 4032 and CECT 5873 strains. The two structures and their temporal evolution were clearly affected by the topography of the surfaces and by the motility. This resulted in a delay in biofilm development on smoother surfaces (AISI 316 SS) and cell grouping in the presence of clefts (AISI 304 SS). The number and size of clusters may be conditioned by motility as well as by the synchrony of the attachment and detachment processes.

Average diffusion distance, covered area and spatio-temporal population distribution, proposed here, were the most informative parameters for quantifying the evolution of biofilm structure.

These results confirm the advantage of image analysis for quantitative characterization of the spatio-temporal evolution of biofilm structures as compared with classical microbiological methods.

6. ACKNOWLEDGEMENTS

This research was funded by the Spanish MINECO (ENZYMONO, AGL2010-22212-C02-02). M. Mosquera-Fernández acknowledges financial support from the JAE-CSIC programme. P. Rodríguez-López acknowledges financial support from the FPI programme. All the authors acknowledge the collaboration Ana Belén Carrera Iglesias (Laboratory technician of MTPM group, IIM-CSIC), Juan Ignacio Molina Rodríguez (BioProcess Engineering group, IIM-CSIC); Mr. Romain Briandet and Mª del Pilar Sanchez Vizuete and the team of B2HM group of Micalis UMR INRA AgroParisTech (Massy, France).

7. REFERENCES

An, Y.H., Friedman, R.J., 2000. Handbook of bacterial adhesion: principles, methods and applications. Humana Press Inc. Towata, New Jersey.

Beyenal, H., Lewandowski, Z., Harkin, G., 2004. Quantifying biofilm structure: facts and fiction. Biofouling 20, 1-23.

Blackman, I.C., Frank, J.F., 1996. Growth of *Listeria monocytogenes* as a biofilm on various food-processing surfaces. Journal of Food Protection 59, 827-831.

Borucki, M.K., Peppin, J.D., White, D., Loge, F., Call, D.R., 2003. Variation in biofilm formation among strains of *Listeria monocytogenes*. Applied and Environmental Microbiology 69, 7336-7342.

Bremer, P.J., Monk, I., Butler, R., 2002. Inactivation of *Listeria monocytogenes*/*Flavobacterium* spp. biofilms using chlorine: impact of substrate, pH, time and concentration. Letters in Applied Microbiology 35, 321-325.

Bridier, A., Dubois-Brissonnet, F., Boubetra, A., Thomas, V., Briandet, R., 2010. The biofilm architecture of sixty opportunistic pathogens deciphered using a high throughput CLSM method. Journal of Microbiological Methods 82, 64-70.

Carpentier, B., Chassaing, D., 2004. Interactions in biofilms between *Listeria monocytogenes* and resident microorganisms from food industry premises. International Journal of Food Microbiology 97, 111-122.

Chae, M.S., Schraft, H., 2000. Comparative evaluation of adhesion and biofilm formation of different *Listeria monocytogenes* strains. International Journal of Food Microbiology 62, 103-111.

Chavant, P., Martinie, B., Meylheuc, T., Bellon-Fontaine, M-N., Hebraud, M., 2002. *Listeria monocytogenes* LO28: surface physicochemical properties and ability to form biofilms at different temperatures and growth phases. Applied and Environmental Microbiology 68, 728-737.

Center for Disease Control and Prevention (CDC), 2014. National Center for Emerging and Zoonotic Infectious Diseases (NCEZID), Division of Foodborne, Waterborne, and Environmental Diseases (DFWED). Avaliable at http//www.cdc.gov/Listeria/outbreaks/index.html. Acceded 10 March 2014.

Daims, H., Wagner, M., 2007. Quantification of uncultured microorganisms by fluorescence microscopy and digital image analysis. Applied Microbiology and Biotechnology 75, 237-248.

Djordjevic, D., Wiedmann, M., McLandsborough, L.A., 2002. Microtiter plate assay for assessment of *Listeria monocytogenes* biofilm formation. Applied and Environmental Microbiology 68, 2950-2958.

342 Edwards, K.J., Rutenberg, A.D., 2001. Microbial response to surface microtopography: the role of
343 metabolism in localized mineral dissolution. Chemical Geology 180, 19-32.

344 European Food Safety Authority (EFSA), European Centre for Disease Prevention and Control (ECDC),
345 2013. The European Union Summary Report on Trends and Sources of Zoonoses and Zoonotics Agents
346 and Food-borne Outbreaks in 2011. EFSA Journal 11, 3129.

347 European Food Safety Authority (EFSA), European Centre for Disease Prevention and Control (ECDC),
348 2014. The European Union Summary Report on Trends and Sources of Zoonoses and Zoonotics Agents
349 and Food-borne Outbreaks in 2012. EFSA Journal 12, 3547.

350 Guggenbichler, J.K., Eberhardt, N., Martinez, H.P., Wildner, H., 2007. Substance with an antimicrobial
351 effect. PCT/EP2007/009814

352 Herrera, J.J.R., Cabo, M.L., Gonzalez, A., Pazos, I., Pastoriza, L., 2007. Adhesion and detachment
353 kinetics of several strains of *Staphylococcus aureus* subsp. aureus under three different experimental
354 conditions. Food Microbiology 24, 585-591.

355 Heubner, E.W., 2009. Stainless Steel- When Health Comes First. Environmental and Human Heath Series
356 2, 1-36.

357 Heydorn, A., Ersboll, B.K., Hentzer, M., Parsek, M.R., Givskov, M., Molin, S., 2000a. Experimental
358 reproducibility in flow-chamber biofilms. Microbiology 146, 2409-2415.

359 Heydorn, A., Nielsen, A.T., Hentzer, M., Sternberg, C., Givskov, M., Ersboll, B.K., Molin, S., 2000b.
360 Quantification of biofilm structures by the novel computer program COMSTAT. Microbiology 146,
361 2395-2407.

362 Ivanenko, Y.V., Lebovka, N.I., Vygornitskii, 1999. Eden growth model for aggregation of charged
363 particles. European Physical Journal B 11, 469-480.

364 Kalmokoff, M.L., Austin, J.W., Wan, G.S., Banerjee, S., Farber, J.M., 2001. Adsorption, attachment and
365 biofilm formation among isolates of *Listeria monocytogenes* using model conditions. Journal of Applied
366 Microbiology 91,725-734.

367 Korber, D.R., Lawrence, J.R., Hendry, M.J., Caldwell, D.E., 1993. Analysis of spatial variability within
368 Mot+ and Mot- *Pseudomonas fluorescens* biofilms using representative elements. Biofouling 7, 339-358.

369 Lau, L., Sanz, M., Herrera, D., Morillo, J.M., Martín, C., Silva, A., 2004. Quantitative real-time
370 polymerase chain reaction versus culture: a comparison between two methods for the detection and
371 quantification of *Actinobacillus actinomycetemcomitans*, *Porphyromonas gingivalis* and *Tannerella*
372 *forsythensis* in subgingival plaque samples. Journal of Clinical Periodontology 31, 1061-1069.

373 Lundén, J.M., Miettinen, M.K., Autio, T.J., Korkeala, H.J., 2000. Persistent *Listeria monocytogenes*
374 strains show enhanced adherence to food contact surface after short contact times. Journal of Food
375 Protection 63, 1204-1207.

376 Ma, H., Bryers, J.D., 2010. Non-invasive method to quantify local bacterial concentrations. Journal of
377 Industrial Microbiology and Biotechnology 37, 1081-1089.

378 Manz, W., Wendt-Potthoff, K., Neu, T.R., Szewzyk, U., Lawrence, J.R., 1999. Phylogenetic
379 Composition, Spatial Structure, and Dynamic of Lotic Bacterial Biofilms Investigated in Situ Hybridation
380 and Confocal Laser Scanning Microscopy. Microbial Ecology 37, 225-237.

381 Marsh, E.J., Luo, H., Wang, H., 2003. A three-tiered approach to differentiate *Listeria monocytogenes*
382 biofilm-forming abilities. FEMS Microbiology Letters 228, 203-210.

383 Miettinen, M.K., Björkroth, K.J., Korkeala, H.J., 1999. Characterization of *Listeria monocytogenes* from
384 an ice cream plant by serotyping and pulsed-field gel electrophoresis. International Journal of Food
385 Microbiology 46, 187-192.

386 Moreto, T., Langsrud, S., 2004. *Listeria monocytogenes*: biofilm formation and persistence in food-
387 processing environments. Biofilms 1, 107-121.

388 Perni, S., Aldsworth, T.G., Jordan, S.J., Fernandes, I., Barbosa, M., Sol, M., Tenreiro, R.P., Chambel, L.,
389 Zilhão, I., Barata, B., Adrião, A., Faleiro, M.L., Andrew, P.W., Shama, G., 2007. The resistance to
390 detachment of dairy strains of *Listeria monocytogenes* from stainless steel by shear stress is related to the
391 fluid dynamic characteristics of the location of isolation. International Journal of Food Microbiology 116,
392 384-390

393 Rieu, A., Briandet, R., Habimana, O., Garmyn, D., Guzzo, J., Piveteau, P., 2008. *Listeria monocytogenes*
394 EGD-e biofilms: no mushrooms but a network of knitted chains. Applied and Environmental
395 Microbiology 74, 4491-4497.

396 Rodríguez, A., Autio, W.R., McLandsborough, L.A., 2008. Effect of surface roughness and stainless steel
397 finish on *Listeria monocytogenes* attachment and biofilm formation. Journal of Food Protection 71, 170-
398 175.

399 Ronner, A.B., Wong, A.C.L., 1993. Biofilm development and sanitizer inactivation of *Listeria*
400 *monocytogenes* and *Salmonella typhimurium* on stainless steel and buna-n-rubber. Journal of Food
401 Protection 56, 750-758.

402 Silva, S., Teixeira, P., Oliveira, R., Azeredo, R., 2008. Adhesion to and viability of *Listeria*
403 *monocytogenes* on food contact surfaces. Journal of Food Protection 71, 1379-1385.

404 Sofos, J.N., 2008. Germ warfare: *Listeria monocytogenes*, enemy No. 1 for the ready-to-eat industry. The
405 National Provisioner, Troy, Michigan.

406 Stepanovic´, S., Vukovic´, D., Dakic´, I., Savic´, B., Sˇvabic´-Vlahovic, M., 2000. A modified microtiter-
407 plate test for quantification of staphylococcal biofilm formation. Journal of Microbial Methods 40, 175-
408 179.

409 Takhistov, P., George, B., 2004. Linearized kinetic model of *Listeria monocytogenes* biofilm growth.
410 Bioprocess and Biosystems Engineering 26, 259-270.

411 Tawakoli, P.N., Al-Ahmad, A., Hoth-Hanning, W., Hanning, M., Hanning, C., 2013. Comparison of
412 different live/dead staining for detection and quantification of adherent microorganisms in the initial oral
413 biofilm. Clinical Oral Investigations 17, 841-850.

414 Todhanakasem, T., Young, G.M., 2008. Loss of flagellum-based motility by *Listeria monocytogenes*
415 results in formation of hyperbiofilms. Journal of Bacteriology 190, 6030-6034.

416 Vatanyoopaisarn, S., Nazli, A., Dodd, C.E.R., 2000. Effect of flagella on initial attachment to *Listeria*
417 *monocytogenes* to stainless steel. Applied and Environmental Microbiology 66, 860-863.

418 Verran, J., Rowe, D.L., Boyd, R.D., 2001. The effect of nanometer dimension topographical features on
419 the hygienic status of stainless steel. Journal of Food Protection 64, 1183-1187.

420 Wakimoto, N., Nishi, J., Sheikh, J., Nataro, J.P., Sarantuya, J., Iwashita, M., Manago, K., Tokuda, K.,
421 Yoshinaga, M., Kawano, Y., 2004. Quantitative biofilm assay using a microtiter plate to screen for
422 enteroaggregative *Escherichia coli*. The American Journal of Tropical Medicine and Hygiene 71. 687-
423 690.

424 Yang, X., Beyenal, H., Harkin, G., Lewandowski, Z., 2000. Quantifying biofilm structure using image
425 analysis. Journal of Microbiological Methods 39, 109-119.

426 Zang, T., Fang, H.H.P., 2001. Quantification of extracellular polymeric substances in biofilms by
427 confocal laser scanning microscopy. Biotechnology Letters 23, 405-409.

428

Figure legends

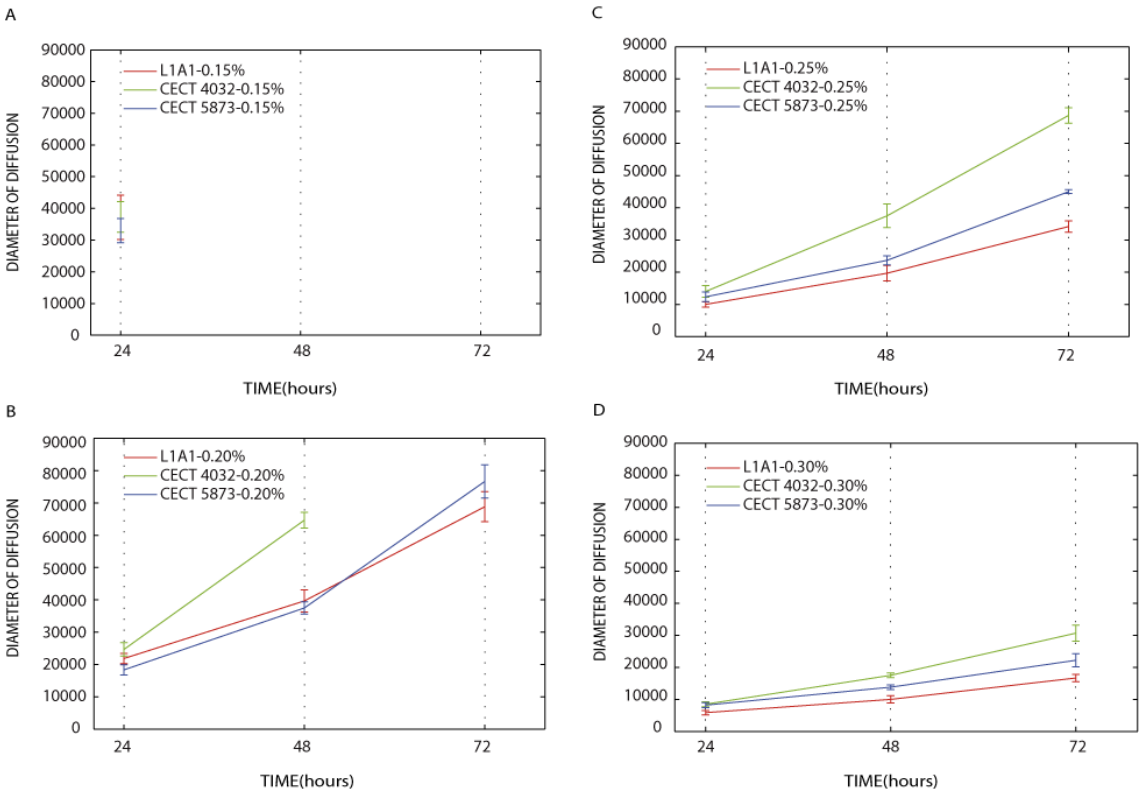

Figure 1. Results of motility test in media with A: 0.15% of agar, B: 0.20% of agar, C: 0.25% of agar and D: 0.30% of agar. Results reflect differences in motility among strains, presenting CECT 4032 strain the highest motile capability and a descendent capability through the time the L1A1 strain, reaching the lowest values in the test.

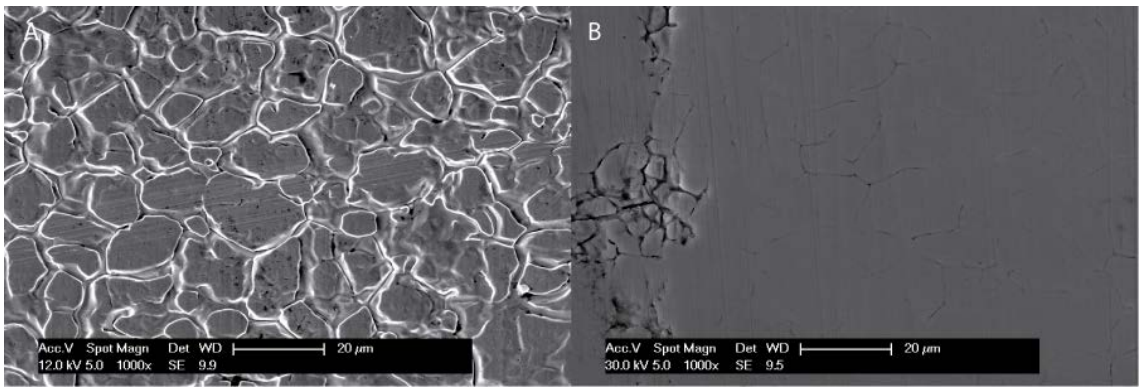

Figure 2. SEM micrographs of (A) AISI 304 SS and (B) AISI 316 SS surfaces. Micrographs show remarkable differences in surface topography among both support types by use of SE detector. AISI 304 SS micrograph presents deep clefts forming pseudo-geometric patterns and AISI 316 SS micrograph shows smooth crevices.

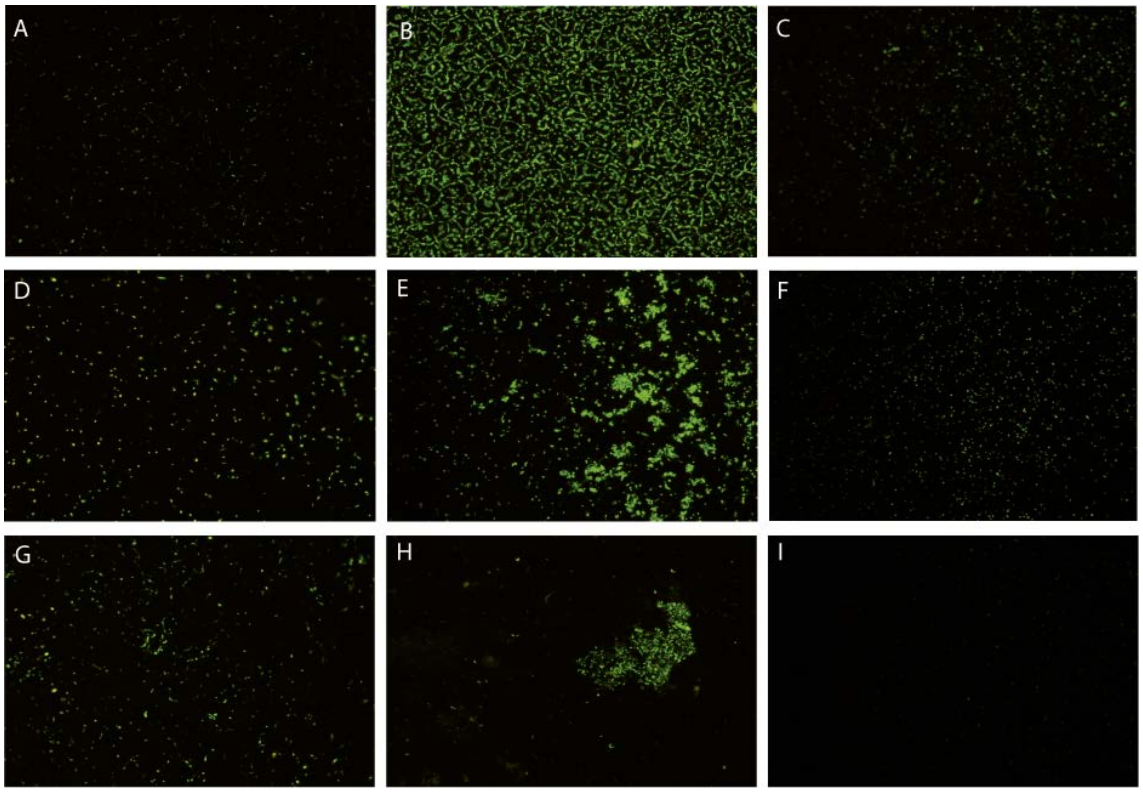

Figure 3. Epifluorescence images of all strains studied on AISI 304 SS, showing the distribution of adherent cells at different sampling times. L1A1 biofilms are showed at A: 72h, B: 96h and C: 240h. L1A1 biofilm image at 96h presents a homogenous layer biofilm that shows net-like pattern. CECT 4032 biofilms in D: 72h, E: 168h and F: 240h images, exhibit at 168h small clusters of viable cells. CECT 5873 biofilms presented in G: 72h, H: 144h and I: 240h images show at 144h large clusters surrounded by individual cells. Biofilms of all strains present similar patterns at 72h and 240h, consisting in individual and viable cells well distributed on surface in a greater or a lesser extent.

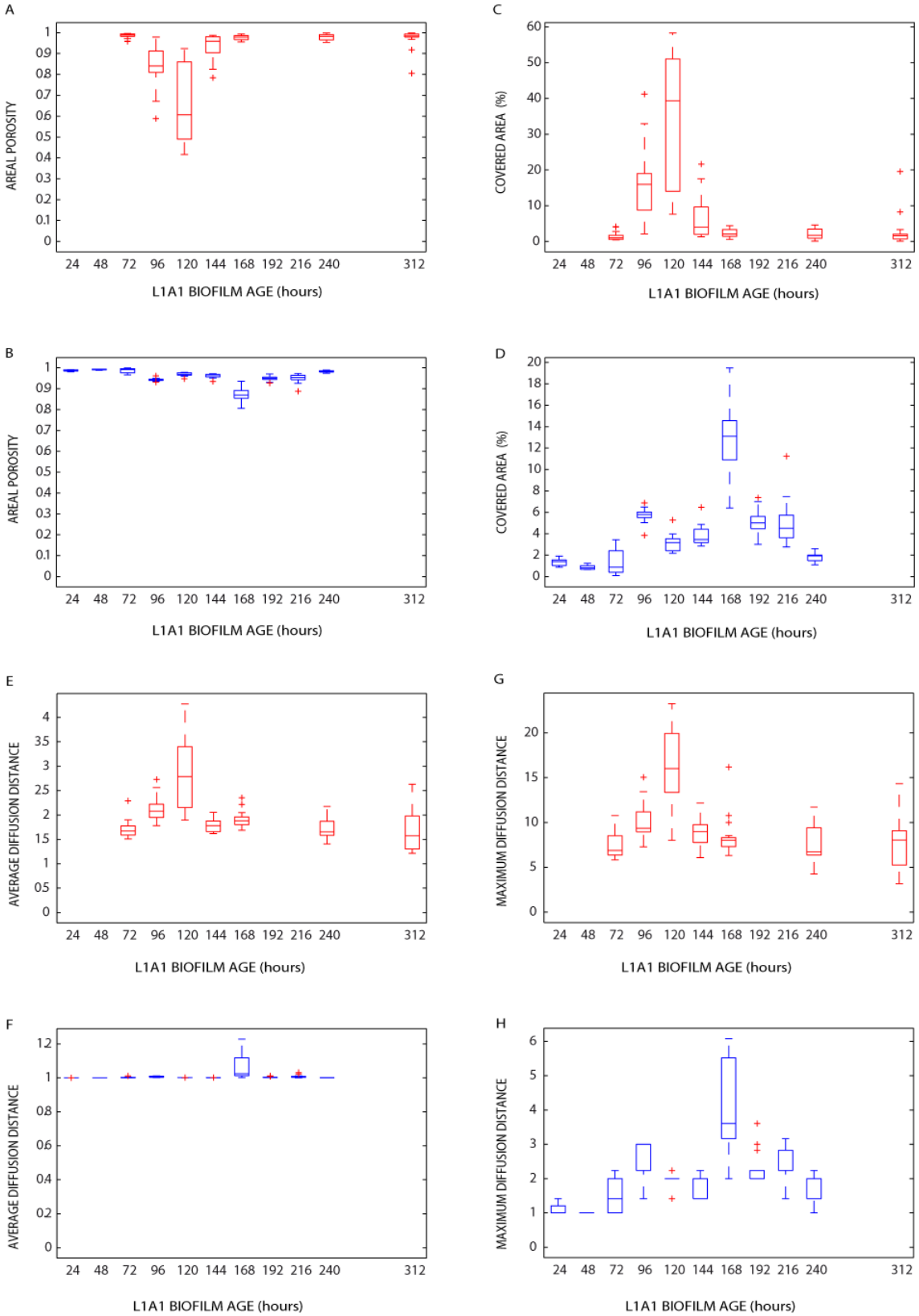

Figure 4. AP (A, B), covered area (C, D), ADD (E, F) and MDD (G, H) obtained from epifluorescence images of L1.A1 biofilms on AISI 304 SS (red) and AISI 316 SS (blue). Structural parameters reflect the formation of a dense biofilm. Structural parameters values obtained from biofilms formed in AISI 316 SS (blue) are clearly lower than those obtained on AISI 304 SS (red).

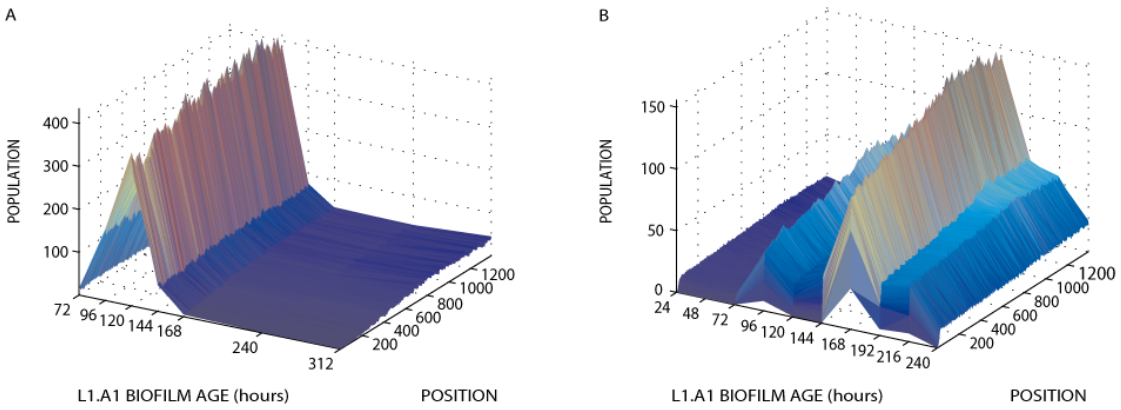

Figure 5. Spatio-temporal Population Distributions obtained from epifluorescence images of L1.A1 biofilms on AISI 304 SS (A) and AISI 316 SS (B). The homogeneous distribution of cells observed at 72 h, 96 h and 240 h on AISI 304 SS reflect the biofilm status exemplified at the images shown in Figure 3 (A, B, C).

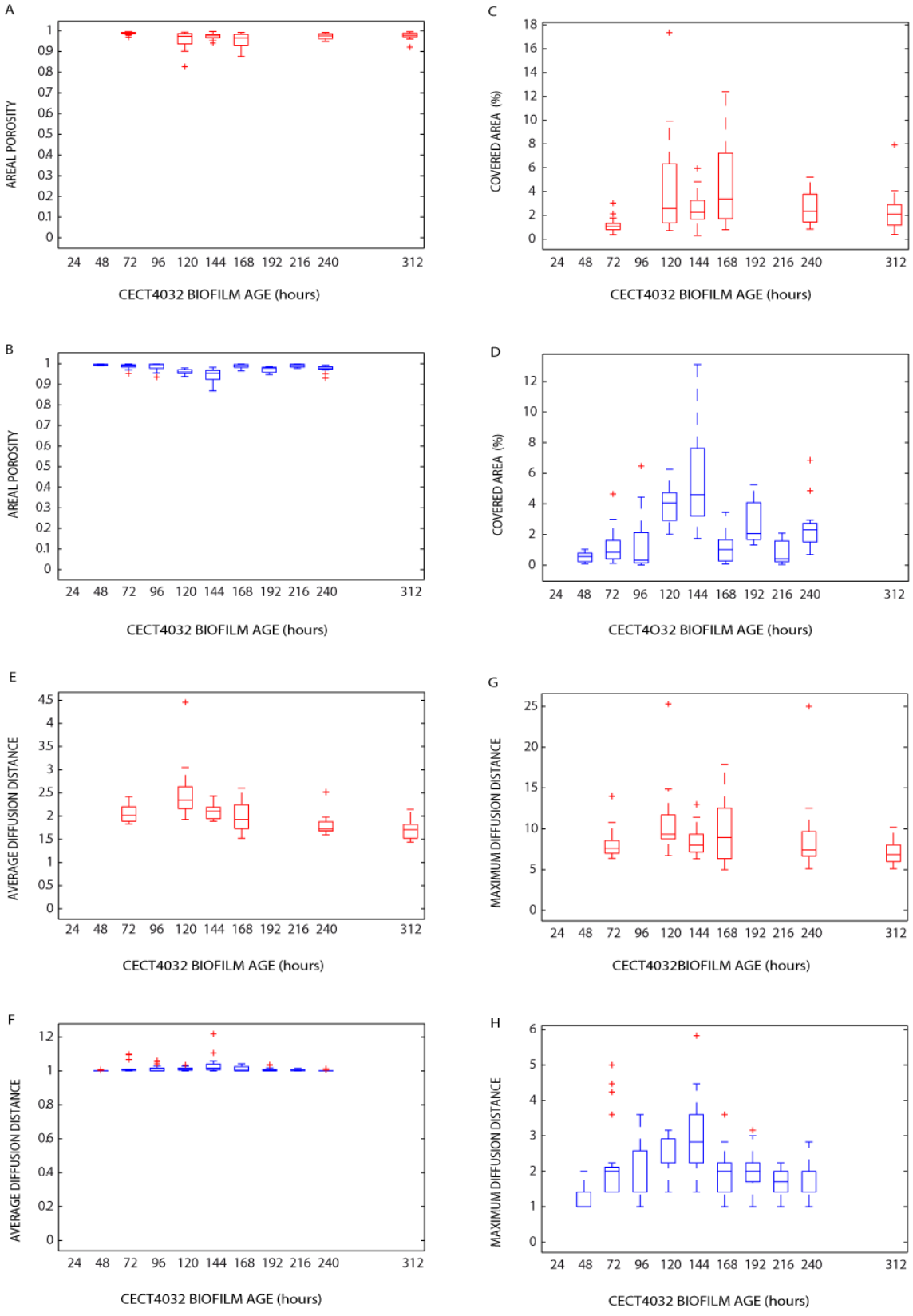

Figure 6. AP (A, B), covered area (C, D), ADD (E, F) and MDD (G, H) obtained from epifluorescence images of CECT 4032 biofilms on AISI 304 SS (red) and AISI 316 SS (blue). Structural parameters reflect the presence of clusters as can also be seen in Figure 3E.

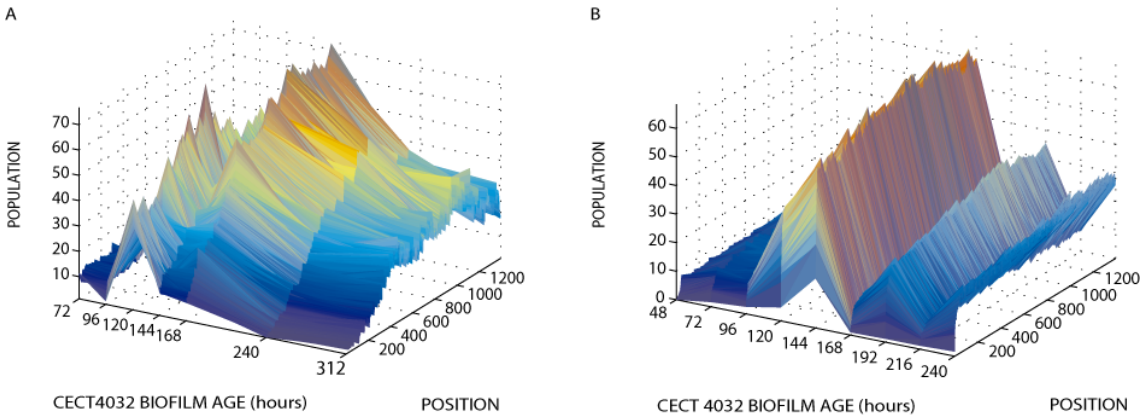

Figure 7. Spatio-temporal Population Distributions obtained from epifluorescence images of CECT 4032 biofilms on AISI 304 SS (A) and AISI 316 SS (B). The distribution of cells at 72 h, 168 h and 240 h on AISI 304 SS reflect the biofilm status exemplified at the images shown in Figure 3(D, E, F). The peaks of different heights at 168 h correspond to presence of aggregates as those shown in Figure 3E.

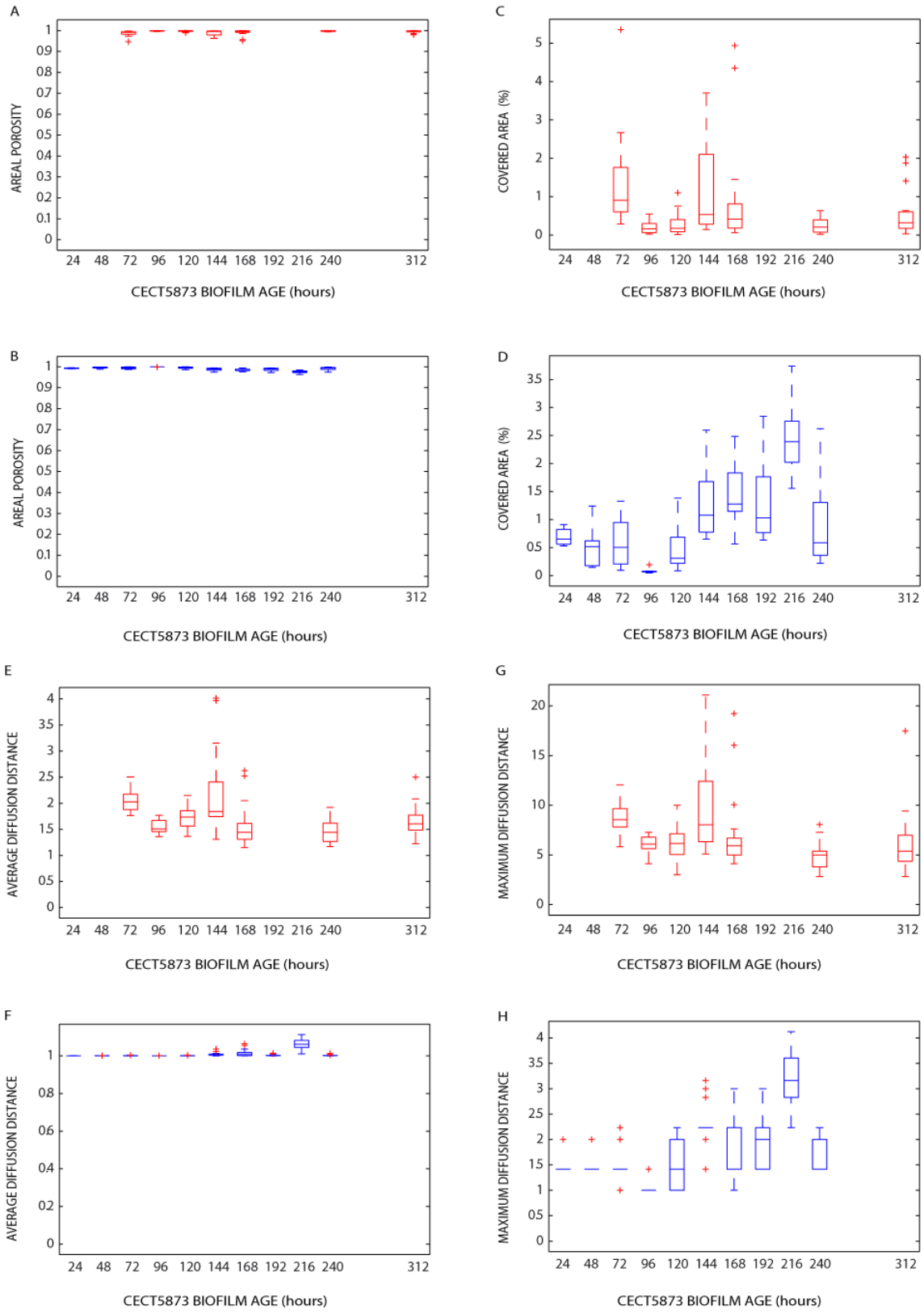

Figure 8. AP (A, B), covered area (C, D), ADD (E, F) and MDD (G, H) obtained from epifluorescence images of CECT 5873 biofilms on AISI 304 SS (red) and AISI 316 SS (blue). Structural parameters reflect the presence of clusters as can also be seen in Figure 3H.

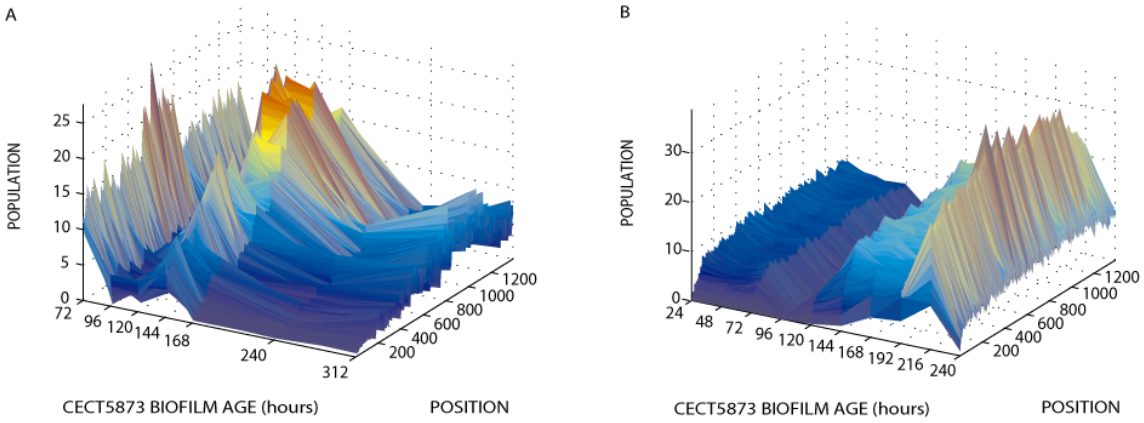

Figure9. Spatio-temporal Population Distributions obtained from epifluorescence images of CECT 5873 biofilms on AISI 304 SS (A) and AISI 316 SS (B). The distribution of cells at 72 h, 144 h and 240 h on AISI 304 SS reflect the biofilm status exemplified at the images shown in Figure 3 (G, H, I). The isolated peak at 144 h corresponds to the presence of large isolated clusters as seen in Figure 3H.

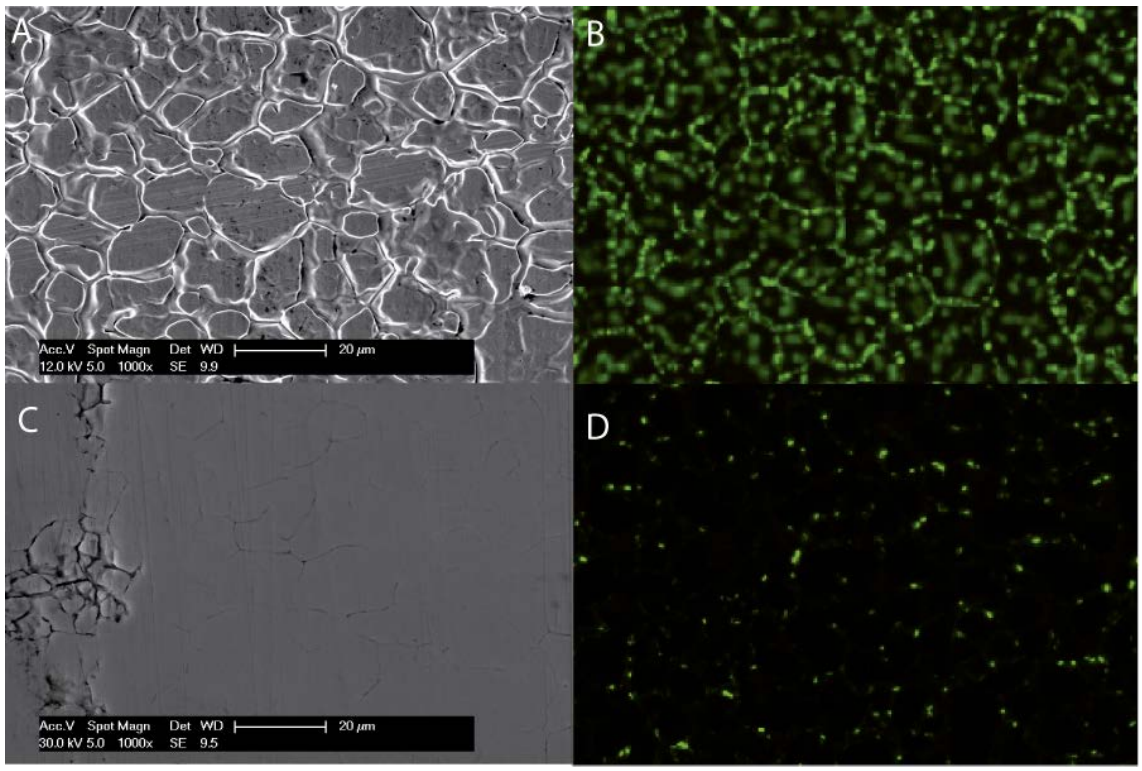

Figure 10. Structural differences in L1.A1 biofilm structure derived from surface topography influence. SEM micrograph of AISI 304 SS (A). L1.A1 biofilm grown on AISI 304 SS (B). SEM micrograph of AISI 316 SS support type (C). L1.A1 biofilm grown on AISI 316 SS (D). L1.A1 biofilms presented cell distribution affected by surface topography, forming chains along the grain boundary in AISI 304 SS surface, in contrast to those structures formed in the smoother AISI 316 SS support.